

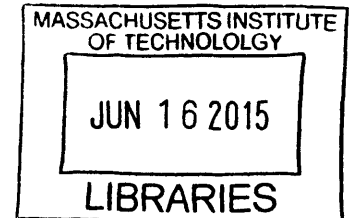
Carbon Nanotube-based Sensors for Label-free Protein Detection

By

Justin T. Nelson

Bachelor of Chemical Engineering
University of Minnesota, 2012

ARCHIVES



Submitted to the Department of Chemical Engineering
in Partial Fulfillment of the Requirements for the Degree of

Master of Science in Chemical Engineering
at the

MASSACHUSETTS INSTITUTE OF TECHNOLOGY

FEBRUARY 2015

© 2015 Massachusetts Institute of Technology. All rights reserved.

Signature redacted

Signature of Author:.....

.....
Department of Chemical Engineering
October 31, 2014

Signature redacted

Certified by:.....

.....
Michael S. Strano
Professor of Chemical Engineering
Thesis Supervisor

Signature redacted

Accepted by:.....

.....
Patrick S. Doyle
Professor of Chemical Engineering
Chairman, Committee for Graduate Students

Carbon Nanotube-based Sensors for Label-free Protein Detection

By

Justin T. Nelson

Submitted to the Department of Chemical Engineering
on October 31, 2014 in Partial Fulfillment of the Requirements for the Degree of
Master of Science in Chemical Engineering

ABSTRACT

Optical biosensors based on fluorescent single-walled carbon nanotubes (SWNT) are a promising alternative to conventional biosensors due to the exceptional photophysical properties of SWNT. Such sensors can enable highly-sensitive, selective, and real-time detection of biological analytes. However, important questions regarding sensor fabrication and reproducibility must be addressed for these sensors to be of practical value. Herein we describe the use of highly-purified, single-chirality SWNT which are functionalized for antibody detection, and demonstrate that reproducibility is drastically improved with these SWNT. Further, we observe a concentration dependence of the effective equilibrium dissociation constant, $K_{D,eff}$, which is in good agreement with previous reports, yet has eluded mechanistic description due to complexities associated with multivalent interactions. We show that a bivalent binding mechanism is able to describe this concentration dependence of $K_{D,eff}$ which varies from 100 pM to 1 uM for IgG concentrations from 1 ng/ml to 100 ug/ml, respectively. The mechanism is shown to describe the unusual concentration-dependent scaling demonstrated by other sensor platforms in the literature, and a comparison is made between resulting parameters. The platform is then extended to the detection of human growth hormone (hGH) using SWNT functionalized with a native hGH receptor (hGH-R), with potential use as a real-time and label-free measurement of protein activity. Native hGH is detected in the micromolar range, and an invariant equilibrium dissociation constant of 9 uM is revealed upon fitting the calibration curve to a single-site adsorption model. Selective detection of native hGH over thermally denatured hGH is shown at a concentration which is 1% of a clinical dose. Lastly, a multichannel detector was built to demonstrate real-time characterization of multiple protein properties. This work could find broad impact in biomanufacturing as real-time analysis of complex biologics is a long-standing goal in this field.

Thesis Supervisor: Michael S. Strano
Title: Professor of Chemical Engineering

TABLE OF CONTENTS

Introduction.....	7
Background.....	8
Sensor Platform Development.....	9
Antibody Detection.....	10
Effective K_D Analysis.....	12
A Bivalent Mechanism.....	15
hGH Activity Assay.....	21
Univalent Binding Model.....	23
Selective Detection of Native hGH.....	25
Instrumentation Development.....	26
Conclusion.....	28
Materials and Methods.....	28
References.....	31

ACKNOWLEDGEMENTS

First and foremost I want to thank my girlfriend, Jordan, for all the love and support during my time at MIT. You have been my best friend through it all, and you continue to amaze me with your endless patience and optimism. You somehow always manage to keep me balanced, even on the tough days when I really don't feel like talking about my day. These have been some of our best and most fun years, and I can't wait for the next chapter of our lives. I also need to thank my parents, Joe and Arlene, and my sister, Amanda, for the unwavering love and confidence in me. Ever since I was a kid, you always encouraged me just to do my best and pursue whatever makes me happy. Many years later you still give me the same great advice, and I couldn't be happier with the results. I am so blessed to have such a loving family. Thank you so much for everything.

Next, I want to express my sincerest gratitude to my advisor, Professor Michael Strano. Your enthusiasm for science is unmatched, and through it you inspired my own passion for research when I first joined the lab. Even as a new student, you had confidence in me and encouraged me to fearlessly tackle hard problems in new fields. I never had to convince you to let me try something new; you always supported my ideas and helped me to develop them, and gave me even more ideas of your own. I have no doubt that my time in your group will have a lasting effect on my life and career, and for that I will always be grateful.

I also need to thank the entire Strano group. You are incredibly unique and talented people, and working with each of you has been a true pleasure. In particular, I want to thank Geraldine Paulus and Nigel Reuel. I am so fortunate to have learned from both of you after joining the SRG, and I hope I was able to help you in the final chapters of your PhDs. I also want to thank Sebastian Kruss, Gili Bisker, Qing Hua Wang, Jiyoung Ahn, and Nicole Iverson for all the knowledge you shared with me and great discussions we had; Kevin Tvrdy, Chih-Jen Shih, Sayalee Mahajan, Youngwoo Son, Zack Ulissi, Lee Draushuk, Seonyeong Kwak, Kumar Varoon Agrawal, and Pingwei Liu for being such friendly, knowledgeable people and answering so many of my questions; Sojin Kim for taking on so much towards the end of my time in the lab and helping me graduate as easily as possible; Maria Chan for all the hard work and for teaching me more about being a mentor than I taught you about doing research; Tom McNicholas, Juan Pablo Giraldo, Markita Landry, Steven Shimizu, Rishabh Jain, Darin Bellisario, Sean Faltermeier, Dan Salem, Anton Cottrill, Georgios Katsukis, and Xun Gong for all the ideas, advice, and distractions you provided on a daily basis, and for being even more distracting outside the lab. Most importantly, you have been an awesome team of people that I am lucky to have spent so much of my time with. I could not have imagined a better group, and I wish all of you the absolute best.

Outside of the Strano group, my research was strongly influenced by the entire DARPA BioMOD team. Many thanks to all of the collaborating groups for sharing some of your own expertise with me, and I wish you all nothing but success as the project moves forward. I especially want to thank Paul Barone and Kerry Love for being constant sources of ideas and encouragement.

I also want to acknowledge those who have made my life as a graduate student so much easier- Lisa Morin, Suzanne Maguire, and Joel Dashnaw. I am truly grateful for all you have done for me personally and for making the department such a pleasant place to work.

In addition to the MIT team, I would like to sincerely thank Professor Dan Frisbie and Dr. Wei Xie from the University of Minnesota for giving me my first opportunity to work in a research lab and encouraging me to pursue graduate school.

Finally I am extremely fortunate to have such great friends from outside the lab. To my classmates who struggled through first semester with me- you are amazing people, lifelong friends, and I wish you each the best in your personal and professional lives. To everyone else, especially Tyler Shortsleeve, Liz Nunnelley, and Stephanie Todis, you all have been great friends and have made these last couple of years an amazing time in my life.

Introduction

SWNT possess unique optical and electronic properties¹⁻⁶ which make them an excellent candidate for a variety of sensing applications.⁷⁻⁹ In particular, optical sensors based on fluorescent SWNT are attractive due to the exceptional sensitivity of SWNT fluorescence intensity and wavelength to changes in the SWNT environment as a result of their one-dimensional nature.¹⁰⁻¹⁴ Further, SWNT do not blink or photobleach,^{2,4,15} which is desirable for long term sensing applications.⁷ There has also been significant interest in using SWNT as *in vivo* imaging agents^{10,16-22} since SWNT are fluorescent in the near-infrared window where tissue is highly transparent.

Such sensors have been demonstrated for a number of targets including DNA,²³⁻²⁵ proteins,²⁵⁻²⁸ glycoproteins,²⁹ peptides,^{16,30} neurotransmitters,³¹ sugars,^{10,32-36} and others small molecules.^{11,18,37-42} Many detection mechanisms have been identified, with SWNT wrapping or biofunctionalization often being central to molecular recognition.^{7,8,43} The platform described here (Figure 1) was first introduced by Ahn et al. for protein detection via specific binding to a capture protein which is tethered to the sensor.²⁶ Fluorescent SWNT are wrapped in chitosan, a readily-available polysaccharide known for its stability, resistance to non-specific protein binding, and biocompatibility.⁴⁴ The chitosan-wrapped SWNT are adsorbed to the surface of a highly-porous hydrogel for immobilization, yet still allowing accessibility of large proteins to the sensors. The wrapping is covalently modified to attach NTA groups chelated to divalent metal cations. It has been shown that certain divalent metal cations quench SWNT fluorescence based on their proximity to the SWNT surface.⁴⁵ These same cations can be used as a docking site for polyhistidine-tagged proteins. Docking of a his-tagged capture protein results in a change in SWNT fluorescence intensity by modulating the distance between the cation and the SWNT

surface. Subsequent binding of the target protein to the capture protein causes a further change in fluorescence intensity. This platform takes advantage of the inherent binding affinity and selectivity often found between proteins in nature. Further, in principle it can be used for any protein for which a binding partner exists.

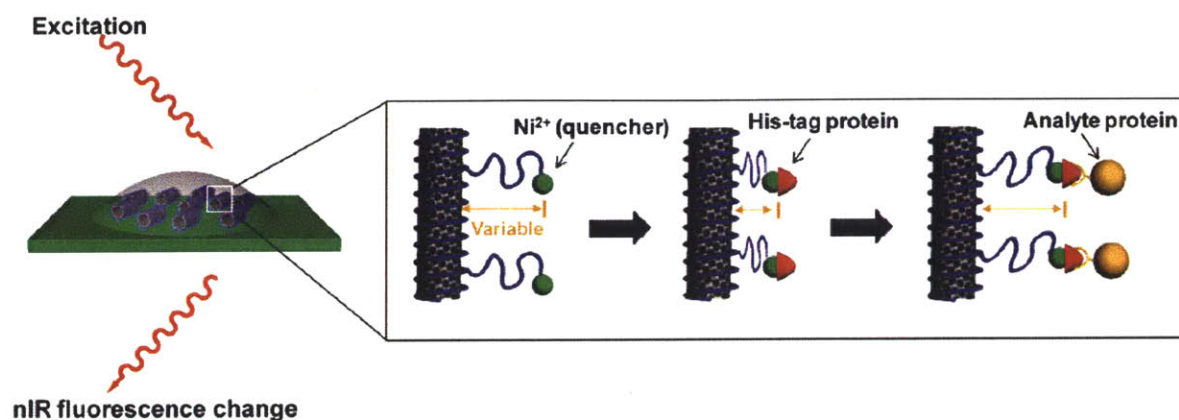


Figure 1. Schematic of detection mechanism. Chitosan-wrapped SWNT are functionalized to display divalent metal cations which modulate SWNT fluorescence based on proximity. The his-tagged capture protein binds to and displaces the metal ion causing a change in fluorescence intensity. Subsequent binding to the analyte protein further displaces the metal ion and modulates fluorescence. Figure adapted from [26].

Background

Early work with this platform focused on qualitative detection of protein-protein interactions.²⁶ A network of 34 proteins expressed via cell-free synthesis were screened against each other to identify binding interactions. SWNT fluorescence intensity was measured using a custom inverted nIR fluorescence microscope. Changes in the fluorescence intensity were indicative of protein binding, and the observed binding pairs were found to match well with previous findings. Subsequent work extended the platform to glycoprotein detection.²⁹ A panel of biotinylated

glycans were conjugated to streptavidin to mimic glycoproteins. Recombinant his-tagged lectins with known carbohydrate recognition domains were used as capture proteins for glycan detection. SWNT fluorescence intensity was monitored over time to capture binding kinetics. The response curves closely resembled sensorgrams obtained from surface plasmon resonance (SPR) or bio-layer interferometry (BLI). A similar analysis was performed using these curves, yielding the forward and reverse rate constants as well as the equilibrium binding constant. For most pairs, the measured kinetic and equilibrium constants were in agreement with constants measured using other platforms. Later work introduced antibody detection,²⁷ using the response from sensor arrays to quantify heterogeneity in an antibody sample. Recombinant his-tagged protein A was used as the capture protein and human IgG as the target protein, as this binding pair is widely used in antibody purification. Polyclonal sources of human IgG demonstrated weaker mean binding affinities and greater variance than monoclonal sources.

Sensor Platform Development

One significant limitation to this technology, as with many emergent biosensor technologies, has been reproducibility. The presence of multiple SWNT chiralities and metallic impurities are known to affect SWNT photoluminescence,⁴⁶ yet unpurified SWNT are often used for sensing purposes. In this work, it was found that using high-purity, single-chirality SWNT drastically improved sensor performance. Sensors prepared from (6,5) SWNT which were first purified to remove other SWNT chiralities and non-SWNT impurities⁴⁷⁻⁵⁰ showed zero failure rate and excellent reproducibility. In contrast, sensors prepared using mixed-chirality SWNT, including (6,5)-enriched CoMoCat SWNT, failed or showed unusual responses in more than half of all experiments. A comparison of the absorbance spectra for CoMoCat and purified (6,5) SWNT

confirms the difference in purity (Figure 2). The spectrum of the purified sample shows a significantly lower baseline absorbance and sharper absorbance peaks, indicative of enhanced purity. The improved sensor performance is attributed to the removal of impurities which can interfere with both the SWNT sensor and the analytes, as many proteins display metal binding domains, and highlights the need to use purified, single-chirality SWNT to reduce sensor variance.

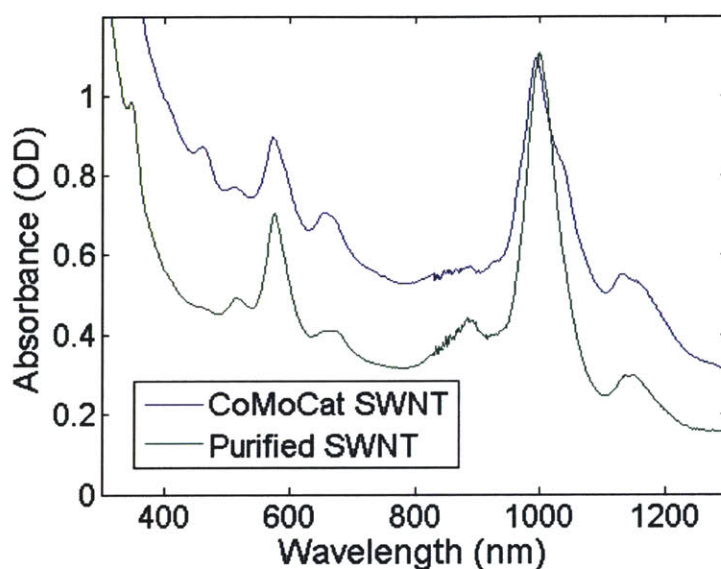


Figure 2. Absorbance spectra of CoMoCat and purified (6,5) SWNT. The baseline absorbance is significantly lower in the purified sample, indicating successful removal of non-SWNT impurities. Absorbance peaks are broader in the CoMoCat sample which is evidence of greater heterogeneity. The improved sensor reproducibility using purified SWNT is attributed to the enhanced purity.

Antibody Detection

This improved detection platform, featuring high-purity, single-chirality SWNT, is demonstrated using antibody detection. Antibodies have emerged as a promising class of biological tools for

therapeutic and diagnostic applications.⁵¹⁻⁵⁵ Affinity chromatography is widely used for antibody recovery and purification, however fundamental questions regarding the binding mechanisms involved in these processes still remain.⁵⁶⁻⁵⁸ For many classes of antibodies, protein A affinity chromatography is chosen due to the high affinity and selectivity protein A has for antibodies such as human IgG. Protein A contains four structurally-similar binding sites with high affinity for the Fc region of most subclasses of human IgG, and the Fc region of human IgG has two sites which can be bound by protein A.⁵⁹

Surface sensors such as SPR and QCM, functionalized to display protein A, are useful tools for immunoassays as they are capable of measuring kinetic and thermodynamic binding parameters. However, as a result of the multivalent nature of both protein A and human IgG, analysis of such binding experiments is complicated and a meaningful interpretation of these parameters has been lacking.⁶⁰ Others have measured apparent equilibrium binding affinities which demonstrate concentration dependence, with significantly greater affinity observed at low human IgG concentrations.^{56,57} This has been generally attributed to the multivalent interactions that are possible at large protein A: IgG ratios, but most techniques lack the sensitivity to measure interactions at very low IgG concentrations. Herein we demonstrate a protein A – modified nIR fluorescent carbon nanotube platform using a Cu^{2+} /NTA/His tag mechanism that we have demonstrated previously^{26,27,29} for real-time, label-free measurement of human IgG binding. With this system, we are able to prepare a calibration curve for picomolar to nearly micromolar IgG concentrations, and measure the dynamics of binding. From these data, we are able to construct a multivalent binding mechanism that are consistent with the kinetics and equilibrium state of binding. The mechanism describes the unusual concentration-dependent scaling

demonstrated by other sensor platforms in the literature, and a comparison is made between resulting parameters.

His-tagged protein A is first loaded onto the sensors which are subsequently exposed to human IgG. Responses to human IgG were measured at concentrations of 100 ug/ml (Figure 3a) to 1 ng/ml, and a limit of detection of 10 ng/ml is achieved. The sensor signal saturates within ~5 minutes at all concentrations, but response magnitudes and kinetics are easily distinguished (Figure 3b).

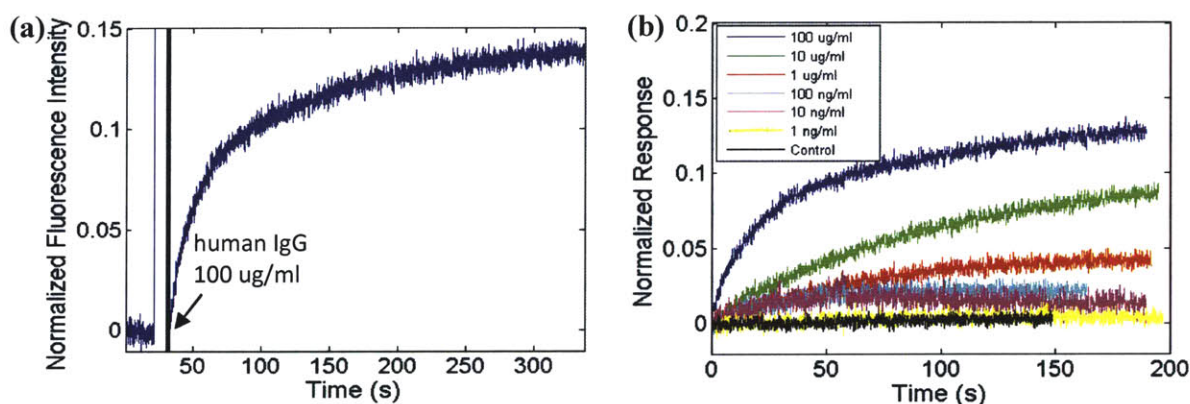
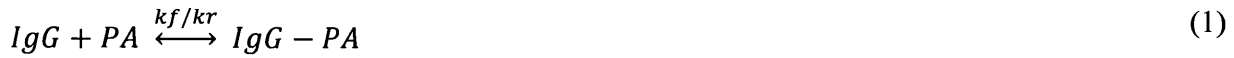


Figure 3. Sensor responses to IgG binding. a) Example binding curve at 100 ug/ml IgG concentration. b) Sensor responses to IgG concentrations from 1 ng/ml to 100 ug/ml. Response magnitudes and kinetics show strong concentration dependences in this range.

Effective K_D Analysis

Several studies of protein A⁵⁶⁻⁵⁸ in the literature employ an effective K_D analysis whereby the binding of such a system is assumed to be monovalent in nature. To determine the effective dissociation constant, $K_{D,eff}$, the response curves are analyzed according to the scheme:



The rate of formation of the bound complex, IgG-PA, is given by

$$\frac{d[IgG - PA]}{dt} = k_f[IgG][PA] - k_r[IgG - PA] \quad (2)$$

The concentration of protein A binding sites is given by

$$[PA] = [PA]_T - [IgG - PA] \quad (3)$$

Substituting (3) into (2) yields

$$\frac{d[IgG - PA]}{dt} = k_f[IgG]([PA]_T - [IgG - PA]) - k_r[IgG - PA] \quad (4)$$

Rearranging (4):

$$\frac{d[IgG - PA]}{dt} = k_f[IgG][PA]_T - k_s[IgG - PA] \quad (5)$$

where

$$k_s = k_f[IgG] + k_r \quad (6)$$

We assume that the concentration of IgG is constant since the amount of IgG is much greater than the number of protein A binding sites. Also, we assume that the change in fluorescence intensity (I) is proportional to the formation of the IgG-PA complex, so (5) can be written:

$$\frac{d(I)}{dt} = k_f[IgG](I_{\max}) - k_s(I) \quad (7)$$

Integrating (7) yields

$$I = \frac{k_f[IgG](I_{max})}{k_f[IgG] + k_r} (1 - e^{-k_s t}) + I_0 \quad (8)$$

The normalized response is then given by

$$R = \frac{I - I_0}{I_{max}} = \frac{k_f[IgG]}{k_f[IgG] + k_r} (1 - e^{-k_s t}) \quad (9)$$

At equilibrium, the exponential term goes to zero and the response is given by

$$R_{eq} = \frac{k_f[IgG]}{k_f[IgG] + k_r} \quad (10)$$

The effective equilibrium dissociation constant is defined as

$$K_{D,eff} = \frac{k_r}{k_f} \quad (11)$$

Substituting (11) into (10):

$$R_{eq} = \frac{[IgG]}{[IgG] + K_{D,eff}} \quad (12)$$

Therefore $K_{D,eff}$ can be calculated from the normalized response:

$$K_{D,eff} = [IgG] \frac{1 - R_{eq}}{R_{eq}} \quad (13)$$

Using (13), $K_{D,eff}$ was calculated for each IgG concentration and is shown in Figure 4b. It is observed that $K_{D,eff}$ strongly depends on IgG concentration, an effect that has been previously reported with other binding platforms. Ogi et al observed dissociation constants of 10^{-11} to 10^{-7} M over a similar range of human IgG concentrations from QCM measurements.⁵⁶ Saha et al. report a dissociation constant of 3.44×10^{-8} M for nanomolar IgG concentrations, but note that higher IgG concentrations do not fit the same K_D as lower concentrations.⁵⁷

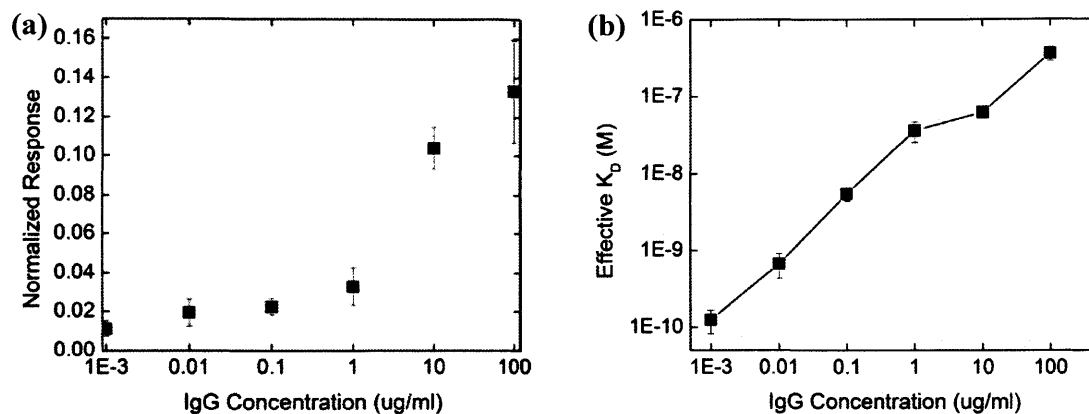


Figure 4. **a)** Calibration curve of the normalized equilibrium responses at each IgG concentration. **b)** Effective K_D measurements showing a strong concentration dependence, with enhanced apparent affinity at lower IgG concentrations.

A Bivalent Mechanism

Protein A forms different binding structures with IgG depending upon the ratio of protein A and IgG present.^{56,57} IgG contains two protein A-binding domains, and protein A contains four IgG-binding domains.^{61,62} However, one can mathematically demonstrate that any number of univalent binding sites on the protein A can be modeled as one average site, without loss of mechanistic description, and yielding a concentration invariant K_D . If we assume protein A has n different univalent binding sites, each with a different dissociation constant, the reaction network is given by n reactions analogous to (14):



The total number of binding sites is:

$$PA + \sum_{i=1}^n IgG - PA_i = PA_T \quad (15)$$

At equilibrium,

$$IgG - PA_i = \frac{[IgG][PA]}{K_{Di}} \quad (16)$$

The normalized sensor response is given by the fraction of bound sites:

$$R_{eq} = \frac{\sum_{i=1}^n IgG - PA_i}{PA_T} = \frac{\sum_{i=1}^n IgG - PA_i}{PA + \sum_{i=1}^n IgG - PA_i} \quad (17)$$

Substituting (16) in (17):

$$R_{eq} = \frac{\sum_{i=1}^n \frac{[IgG][PA]}{K_{Di}}}{PA + \sum_{i=1}^n \frac{[IgG][PA]}{K_{Di}}} \quad (18)$$

As shown in (13), the effective K_D is given by:

$$K_{D,eff} = [IgG] \frac{1 - R_{eq}}{R_{eq}} \quad (19)$$

Substituting (18) in (19):

$$K_{D,eff} = [IgG] \frac{PA}{\sum_{i=1}^n \frac{[IgG][PA]}{K_{Di}}} = \frac{1}{\sum_{i=1}^n \frac{1}{K_{Di}}} \quad (20)$$

From (20), we see that for an arbitrary number of univalent binding sites with different dissociation constants, the effective dissociation constant does not display a concentration dependence. Hence, the concentration dependent K_D necessarily means that the mechanism is multivalent, involving two or more IgG or protein A molecules.

At relatively low IgG concentrations, a single IgG molecule can be bound twice by protein A which results in a larger apparent affinity. At very high IgG concentrations, multiple IgG molecules can bind to a single protein A, resulting in a lower apparent affinity. Therefore the observed dissociation constant does not reflect the formation of a single structure, but the apparent binding constant from a distribution of structures. Since each protein A-binding domain of human IgG can bind once to any of the four IgG-binding domains of protein A with nearly the same affinity, the only true thermodynamic binding constant for this pair is for univalent binding. We first consider this univalent interaction using a single-site adsorption model:



The dissociation constant, K_{D1} , is given by

$$K_{D1} = \frac{[IgG][PA]}{[IgG - PA]} \quad (22)$$

The total number of protein A binding sites is

$$[PA]_T = [PA] + [IgG - PA] \quad (23)$$

$$[PA] = [PA]_T - [IgG - PA] \quad (24)$$

Substituting (24) into (22):

$$[IgG - PA] = \frac{[IgG][PA]_T}{[IgG] + K_{D1}} \quad (25)$$

As shown before, the normalized response is then given by

$$R = \frac{[IgG - PA]}{[PA]_T} = \frac{[IgG]}{[IgG] + K_{D1}} \quad (26)$$

Fitting our data to this univalent binding model indicates that $K_{D1} = 30$ nM (Figure 5a), however it is clear that low IgG concentrations are not fit well by this model. Therefore it is crucial to understand the relationship between univalent and bivalent binding structures, and determine when bivalent structures begin to significantly affect the observed binding constant.

To account for the bivalency of human IgG, we take a probabilistic approach which has been described previously.^{60,63} First, we define a parameter f :

$$f = \text{fraction of bound IgG sites} = \frac{[\text{bound IgG sites}]}{[\text{total IgG sites}]} \quad (27)$$

In our system, the numerator is simply the concentration of IgG-PA structures, [IgG-PA]. The denominator is just $2 \cdot [\text{IgG}]$ since we assume [IgG] is approximately unchanged during the experiment and the valency of IgG is two. Therefore,

$$f = \frac{[\text{IgG} - \text{PA}]}{2[\text{IgG}]} \quad (28)$$

We then assume a binomial distribution between univalent and bivalent binding.

$$\text{fraction of unbound IgG} = (1 - f)^2 \quad (29)$$

$$\text{fraction of univalently bound IgG} = 2f(1 - f) \quad (30)$$

$$\text{fraction of divalently bound IgG} = f^2 \quad (31)$$

Therefore the ratio of univalent to bivalent IgG is:

$$\frac{\text{univalent}}{\text{bivalent}} = \frac{2f(1 - f)}{f^2} = \frac{2}{f} - 2 \quad (32)$$

Substituting (28) and (25) into (32), we can determine the ratio of binding types at any IgG concentration:

$$\frac{\text{univalent}}{\text{bivalent}} = \frac{2}{f} - 2 = \frac{4[\text{IgG}]}{[\text{IgG} - \text{PA}]} - 2 = \frac{4[\text{IgG}]([\text{IgG}] + K_{D1})}{[\text{IgG}][\text{PA}]_T} - 2 \quad (33)$$

So finally:

$$\frac{\text{univalent}}{\text{bivalent}} = \frac{4([\text{IgG}] + K_{D1})}{[\text{PA}]_T} - 2 \quad (34)$$

From (34), we see that at high IgG concentrations (specifically $[\text{IgG}] \sim K_{D1}$), this ratio grows linearly with $[\text{IgG}]$, ultimately leading to a nearly-univalent binding system which is accurately modeled by a single-site adsorption model. However, at low IgG concentrations ($[\text{IgG}] \ll K_{D1}$), we see that the ratio approaches a constant. Therefore the system is governed by a different K_D in this regime, one which incorporates bivalent binding. We previously saw that the univalent binding constant $K_{D1} \sim 30$ nM. Since IgG concentrations were tested from 70 pM to 700 nM, both binding regimes ($[\text{IgG}] \ll K_{D1}$ and $[\text{IgG}] \sim K_{D1}$) were encountered. We conclude that the solution is simply a sum of two independent binding models, as is used elsewhere:⁶⁴

$$R = \frac{a_1[\text{IgG}]}{[\text{IgG}] + K_{D1}} + \frac{a_2[\text{IgG}]}{[\text{IgG}] + K_{D2}} \quad (35)$$

The factors a_1 and a_2 are the normalized capacities for each binding type. Since it is likely that not all binding sites can support bivalent binding due to steric restrictions, we expect that a_2 is less than a_1 . Fitting our data with this solution reveals $a_1=0.1225$, $a_2=0.01802$, $K_{D1}=33$ nM, and $K_{D2}=3.6$ pM (Figure 5b). By inspection, it is clear that low IgG concentrations are fit much better by this model than the simple univalent model. It is noteworthy that the bivalent model is able to describe the low concentration region of the IgG calibration curve. Despite being in the

shallow section of the response curve, the model is able to extend accurate predictions of low IgG concentration, increasing its utility (Fig 5b, inset).

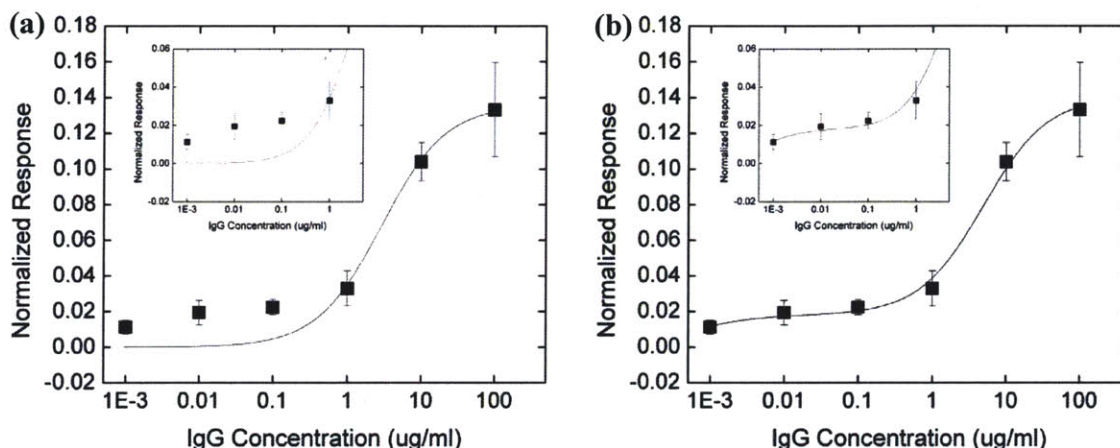


Figure 5. Comparison of human IgG-protein A binding models. **a)** Univalent binding model which suggests $K_{D1} = 30$ nM. When the bivalency of IgG is neglected, the model fails to fit the behavior at low [IgG] (inset). **b)** Bivalent binding model. When the bivalency of IgG is accounted for, the model is able to predict the enhanced affinity observed at low [IgG] (inset) while still fitting the results at high [IgG]. As a result of the bivalency, this model reveals two binding constants: $K_{D1} = 33$ nM and $K_{D2} = 3.6$ pM.

The $K_{D,eff}$ measured on our platform, along with the bivalent binding model, are shown with dissociation constants reported by others in Figure 6. Our results are consistent with previous reports. Ogi et. al. observe a similar concentration dependence, a trend which is approximated by our bivalent model. Saha et. al. and Schwartz et. al. measure similar dissociation constants at relatively high IgG concentrations which validate the results from our detection platform.

Quantitative differences are likely due to source and quality of protein A and human IgG used, as well as the specific experimental conditions.

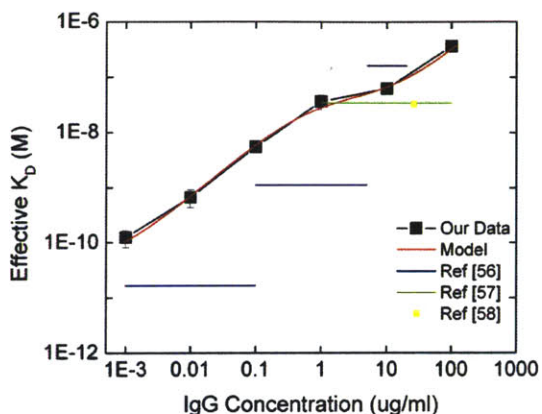


Figure 6. Comparison of K_D measurements between our sensor platform and other platforms featuring immobilized protein A. At large IgG concentrations, all platforms reveal a similar K_D . At lower concentrations, the increased affinity observed by Ogi et. al. is similar to what is observed in our platform. This trend is captured by the bivalent binding model.

hGH Activity Assay

One potential application for this technology is for rapid measurement of drug potency, specifically for biopharmaceutical therapeutics. Techniques assessing protein activity vary based on the particular function of the protein, but often an animal model or cell-based assay is needed. Binding assays can sometimes be used as a surrogate measurement for activity if the assay is designed such that protein binding can be correlated to its activity. Here, we demonstrate quantitative measurement of hGH binding to sensors functionalized with an hGH receptor for use as an activity assay. The standard for determining hGH activity is the hypophysectomized rat weight gain bioassay.⁶⁵⁻⁶⁷ This assay involves measuring the weight gain of hypophysectomized

rats following multiple hGH injections per day for 10 days. Not only is this process time and labor intensive, the results can vary by more than 50%, requiring many replicate measurements to achieve a meaningful result.⁶⁸ Since drug potency measurements are critical to biomanufacturing and pharmaceutical production, efforts have been made to develop assays which are suitable to replace the weight gain assay. These *in vitro* assays are based on measuring hGH binding to the extracellular binding domain of its native receptor (hGH-R) in an attempt to simulate the *in vivo* assay. One such set of assays is based on cellular proliferation of a cell line transfected to display hGH-R on its surface.⁶⁸ Proliferation after exposure to hGH for ~1 day is shown to be dose-dependent with less variance than the weight gain assay. Another set of assays are based on hGH binding to hGH-R in solution and subsequent measurement of the extent of binding through chromatography.⁶⁸ In this case, binding is again shown to be dose-dependent and correlates with the weight gain assay.

In this work, measurement of hGH binding to sensors functionalized with an hGH receptor was performed using the same approach as was used with human IgG. In contrast to the multivalent binding behavior seen with human IgG, we demonstrate monovalent binding using human growth hormone (hGH) as the target analyte. We use a his-tagged extracellular binding domain of the native hGH receptor (hGH-R) as the immobilized binding partner. Sensor fabrication is similar to the his-tagged protein A – human IgG detection platform, with his-tagged hGH-R replacing protein A as the capture protein. Signal transduction is observed upon hGH-R loading and hGH binding. Concentration dependent responses are observed as shown in Figure 7, and the normalized response magnitudes can be used to prepare a calibration curve.

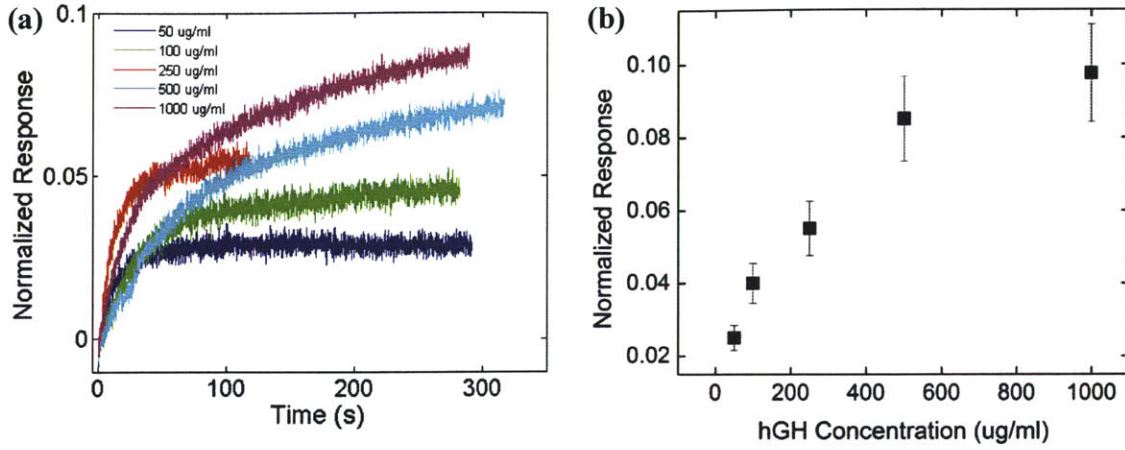


Figure 7. Measurements of hGH binding. a) Sensor responses to hGH concentrations from 50 ug/ml to 1000 ug/ml. Response magnitudes are clearly concentration dependent in this range. The variance in response kinetics is likely due to pipetting variability. b) hGH calibration curve. Four replicate measurements were made at 1000 ug/ml, and this variance was used to estimate the variances at the lower concentrations.

Univalent Binding Model

hGH binding to hGH-R in this system can be modeled by a single-site adsorption model.



$$K_D = \frac{[hGH][hGH - R]}{[hGH:hGH - R]} \quad (37)$$

The concentration of free hGH-R sites is given by

$$[hGH - R] + [hGH:hGH - R] = [hGH - R]_T \quad (38)$$

where $[hGH-R]_T$ is the total concentration of receptor sites. Substituting (38) into (37):

$$K_D = \frac{[hGH]([hGH - R]_T - [hGH:hGH - R])}{[hGH:hGH - R]} \quad (39)$$

The fraction of bound sites is defined as

$$\theta = \frac{[hGH:hGH - R]}{[hGH - R]_T} \quad (40)$$

Substituting (40) into (39):

$$K_D = \frac{[hGH](1 - \theta)}{\theta} \quad (41)$$

Solving for θ :

$$\theta = \frac{[hGH]}{K_D + [hGH]} \quad (42)$$

As was done earlier, we assume that the fraction of bound sites is proportional to the normalized response of our sensors. Fitting (42) using non-linear regression yields $K_D \sim 9 \mu\text{M}$.

Using this single-site adsorption model is only valid if cooperativity does not play a role in binding. Equation (42) can be written in the form of the Hill equation to determine if cooperativity is involved:

$$\theta = \frac{[hGH]^n}{K_D^n + [hGH]^n} \quad (43)$$

where n is the Hill coefficient. If $n=1$, cooperative binding is not occurring and can be neglected.

(43) can be rewritten as

$$\theta = \frac{1}{\left(\frac{K_D}{[hGH]}\right)^n + 1} \quad (44)$$

Inverting and rearranging yields

$$\frac{1 - \theta}{\theta} = \left(\frac{K_D}{[hGH]}\right)^n \quad (45)$$

Inverting again and taking the log of both sides:

$$\log \frac{\theta}{1 - \theta} = n * \log[hGH] - n * \log K_D \quad (46)$$

From (46), plotting $\log(\theta / (1 - \theta))$ versus $\log[hGH]$ should result in a line whose slope is n and intercept is $-n * \log(K_D)$. In Figure 8, we see that the slope is very nearly 1 indicating that

cooperative binding does not play a role and can be neglected. The intercept indicates that $K_D = 8.6 \mu\text{M}$, which is in agreement with the value determined through non-linear regression.

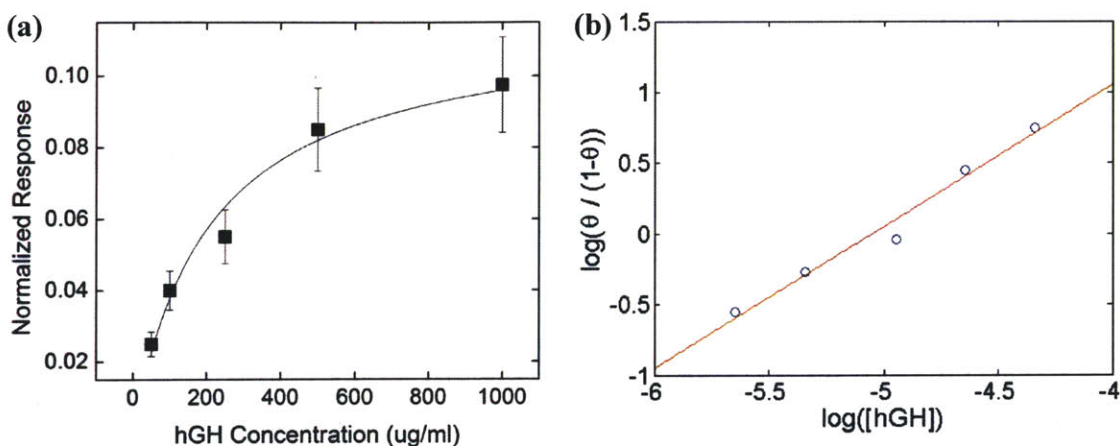


Figure 8. a) hGH calibration curve with a single-site adsorption model, revealing $K_D = 9 \mu\text{M}$. b) Hill plot to determine cooperativity. The slope = 1.00 indicating that cooperativity is not a factor in hGH binding in this system. The intercept = 5.06 yielding $K_D = 8.6 \mu\text{M}$.

Selective Detection of Native hGH

Sample quality can influence the kinetics and extent of binding. As an additional check, hGH was purposely denatured to distinguish active from inactive forms of the same analyte. After heating to $95 \text{ }^\circ\text{C}$ for 20 minutes, complete loss in secondary structure is observed. At the same concentration ($50 \mu\text{g/ml}$), different responses are seen to the native and denatured forms (Figure 9). Both induce a response, but only the response to the native protein is sustained. An initial increase after adding denatured hGH is followed by a drop in signal which appears to be characteristic of weak, non-specific interactions. Distinguishing native and thermally denatured hGH at $50 \mu\text{g/ml}$ is significant since this concentration is approximately 1% of a clinical dose, which is low enough to detect typical hGH variants in drug production.

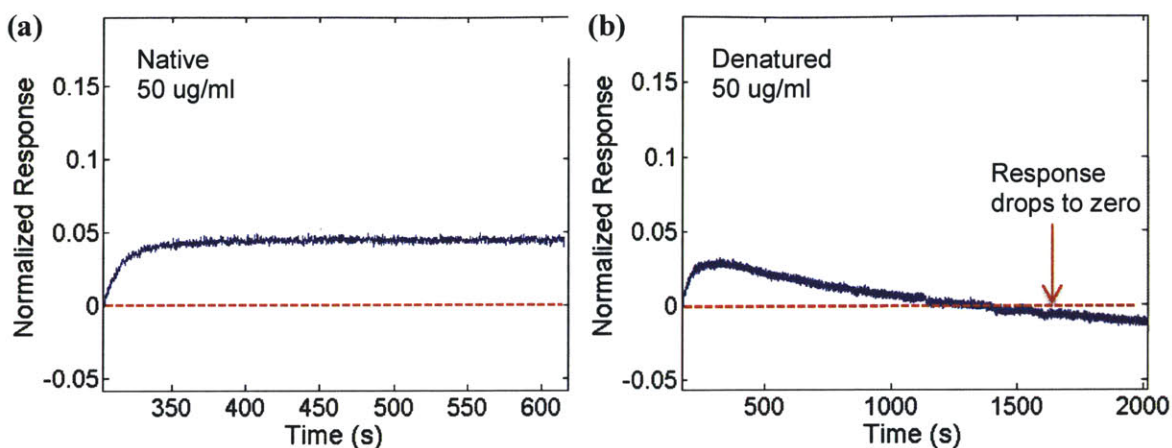


Figure 9. Selective detection of native hGH. a) The response to 50 ug/ml native hGH remains constant over time. b) Exposure to 50 ug/ml thermally denatured hGH results in a temporary response which reduces to zero over time, indicative of weak, non-specific binding.

Instrumentation Development

Lastly, we demonstrate instrumentation which enables multiplexing of this detection platform for simultaneous characterization of multiple protein properties (Figure 10). The optical pathway in this multiplexed instrument is similar to what has been described previously.⁶⁹ A 565nm high-power LED is first filtered and collimated. It passes through a set of three 50/50 beam splitters to create four nearly identical excitation beams. Each excitation beam is directed up towards the sample with an 850 LP dichroic mirror. The beams are focused onto each sample using aspheric condenser lenses. Fluorescent emission follows the same beam path as excitation except it passes through the dichroic mirror and is focused onto InGaAs nIR photodiodes. Each detector outputs a voltage proportional to the fluorescence intensity, and the signal is collected for analysis.

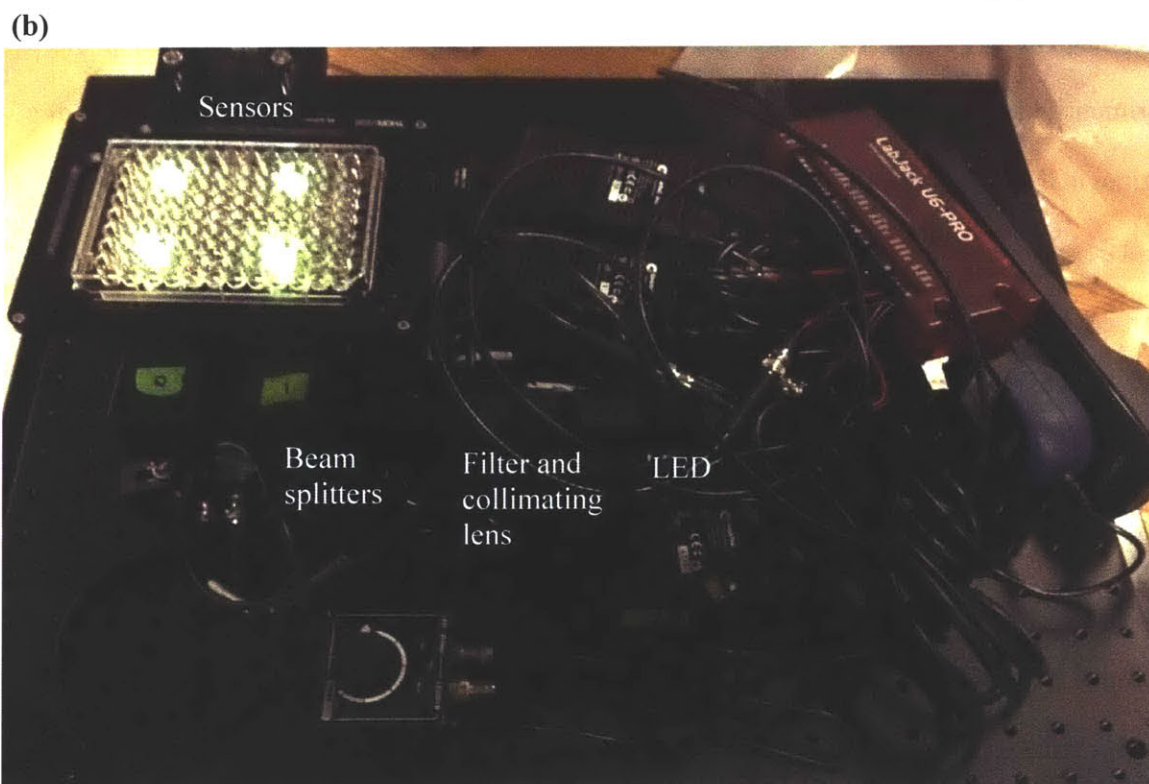
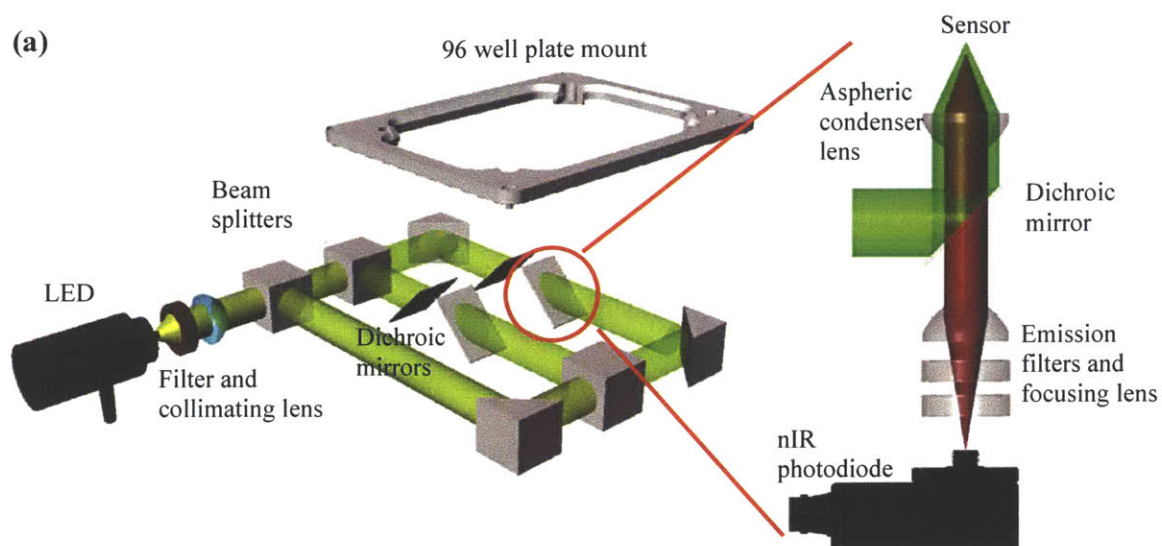


Figure 10. a) Schematic of multichannel SWNT fluorescence detector. A high-power LED is split into four beams. Dichroic mirrors direct each beam to the samples, and aspheric condenser lenses focus the excitation. The fluorescent emission from each sensor passes through the dichroic and is filtered and focused onto a nIR photodiode which outputs a signal to the data

acquisition card. b) Photograph of the multichannel device. The sensors are contained within wells of a well plate which is mounted above the excitation pathway.

Conclusion

Optical biosensors based on fluorescent SWNT have clear advantages for use in protein detection. The speed, sensitivity, and label-free nature of this sensor platform make it an attractive technology for healthcare and biomanufacturing applications. In this work, we have shown significant improvements in sensor reproducibility which is critical for these sensors to be of practical value. Further, we demonstrate that the information obtained from binding experiments can provide mechanistic insight. We apply this technology to the development of a real-time hGH activity assay and demonstrate selective detection of native hGH at 1% of a typical dose. Instrumentation which enables multiplexed detection with this platform is constructed, paving the way for robust, real-time protein characterization.

Materials and Methods

Chitosan-Wrapped SWNT Preparation

High-purity, single-chirality (6,5) SWNT in SDS (purified according to Tvrđy et al⁴⁹) were first exchanged into a chitosan suspension. 15 mL of 5 mg/L SDS-SWNT suspension and 15 mL of methanol were mixed to flocculate the SWNT from suspension. The mixture was then centrifuged at 3200 x g for 15 minutes. The SWNT mass was dispersed in water to wash away residual SDS and methanol. The mixture was centrifuged at 16,000 x g for 15 minutes, and the SWNT mass was collected and dispersed in water again. This process was repeated five times to ensure that all SDS and methanol was removed. After the final centrifugation, the SWNT mass

was transferred to 10 mL of 2.5 mg/mL chitosan in water containing 1 vol% acetic acid. The SWNT were suspended via tip sonication at 10W for 45 minutes. The resulting mixture was centrifuged at 16,000 x g for 1.5 hours to remove SWNT aggregates. The supernatant (containing the stable chitosan-wrapped SWNT suspension) was removed and centrifuged again, and the resulting supernatant was collected.

Sensor Fabrication

First, 2 mg/mL (0.2 wt%) of agarose was melted in water by heating until the solution became clear. Care was taken to avoid boiling. The solution was cooled to ~ 40 °C and 50 uL gel spots were deposited to the bottom of each well of a 96 microwell plate. The gels were cured in a humid environment for 30 minutes. 15 uL of chitosan-wrapped SWNT (5 mg/L) was spot onto each gel. The wells were incubated for 45 minutes in a humidified chamber at 37 °C. They were then removed from the incubator and each well was gently washed with water to remove any excess SWNT solution.

Sensor functionalization was similar to the procedure outlined before.²⁷ First, 5 mg/mL of succinic anhydride in 300 mM PBS was added to each well and incubated overnight. The wells were washed with water. The carboxylic acids were activated with 20 mg/mL EDC and 60 mg/mL NHS in MES buffer for two hours. The wells were again washed with water. Copper-NTA⁷⁰ was then coupled to the NHS esters. The reaction was carried out in a HEPES buffer for 5 hours. The wells were washed with PBS and were ready for testing.

Sensor Testing

Sensors were equilibrated in 180 uL of PBS and loaded with 20 uL of the appropriate his-tagged receptor protein (1 mg/mL protein A for IgG binding, 100 ug/mL hGH-R for hGH binding), as described before.⁶⁹ The well was then washed with PBS to remove excess receptor protein.

Binding was measured as 20 μL of the desired analyte was added to the receptor-functionalized sensor. SWNT fluorescence intensity was monitored for the duration of the experiment to record binding events in real time.

References

- 1 Avouris, P., Freitag, M. & Perebeinos, V. Carbon-nanotube photonics and optoelectronics. *Nat Photon* **2**, 341-350 (2008).
- 2 Bachilo, S. M. *et al.* Structure-Assigned Optical Spectra of Single-Walled Carbon Nanotubes. *Science* **298**, 2361-2366, doi:10.1126/science.1078727 (2002).
- 3 Moore, V. C. *et al.* Individually Suspended Single-Walled Carbon Nanotubes in Various Surfactants. *Nano Letters* **3**, 1379-1382, doi:10.1021/nl034524j (2003).
- 4 O'Connell, M. J. *et al.* Band Gap Fluorescence from Individual Single-Walled Carbon Nanotubes. *Science* **297**, 593-596, doi:10.1126/science.1072631 (2002).
- 5 Strano, M. S. Probing Chiral Selective Reactions Using a Revised Kataura Plot for the Interpretation of Single-Walled Carbon Nanotube Spectroscopy. *Journal of the American Chemical Society* **125**, 16148-16153, doi:10.1021/ja036791x (2003).
- 6 Wang, Q. H. *et al.* Low Dimensional Carbon Materials for Applications in Mass and Energy Transport. *Chemistry of Materials* **26**, 172-183, doi:10.1021/cm402895e (2013).
- 7 Kruss, S. *et al.* Carbon nanotubes as optical biomedical sensors. *Advanced Drug Delivery Reviews* **65**, 1933-1950, doi:<http://dx.doi.org/10.1016/j.addr.2013.07.015> (2013).
- 8 Mu, B. *et al.* Recent Advances in Molecular Recognition Based on Nanoengineered Platforms. *Accounts of Chemical Research* **47**, 979-988, doi:10.1021/ar400162w (2014).
- 9 Boghossian, A. A. *et al.* Near-Infrared Fluorescent Sensors based on Single-Walled Carbon Nanotubes for Life Sciences Applications. *ChemSusChem* **4**, 848-863, doi:10.1002/cssc.201100070 (2011).

- 10 Barone, P. W., Baik, S., Heller, D. A. & Strano, M. S. Near-infrared optical sensors based on single-walled carbon nanotubes. *Nat Mater* **4**, 86-92, doi:http://www.nature.com/nmat/journal/v4/n1/supinfo/nmat1276_S1.html (2005).
- 11 Kim, J.-H. *et al.* The rational design of nitric oxide selectivity in single-walled carbon nanotube near-infrared fluorescence sensors for biological detection. *Nat Chem* **1**, 473-481, doi:http://www.nature.com/nchem/journal/v1/n6/supinfo/nchem.332_S1.html (2009).
- 12 Choi, J. H. & Strano, M. S. Solvatochromism in single-walled carbon nanotubes. *Applied Physics Letters* **90**, 223114-223114-223113, doi:10.1063/1.2745228 (2007).
- 13 Silvera-Batista, C. A., Wang, R. K., Weinberg, P. & Ziegler, K. J. Solvatochromic shifts of single-walled carbon nanotubes in nonpolar microenvironments. *Phys Chem Chem Phys* **12**, 6990-6998, doi:Doi 10.1039/B927053a (2010).
- 14 Tsyboulski, D. A., Bachilo, S. M. & Weisman, R. B. Versatile Visualization of Individual Single-Walled Carbon Nanotubes with Near-Infrared Fluorescence Microscopy. *Nano Letters* **5**, 975-979, doi:10.1021/nl050366f (2005).
- 15 Heller, D. A., Baik, S., Eurell, T. E. & Strano, M. S. Single-Walled Carbon Nanotube Spectroscopy in Live Cells: Towards Long-Term Labels and Optical Sensors. *Advanced Materials* **17**, 2793-2799, doi:10.1002/adma.200500477 (2005).
- 16 Bisker, G., Iverson, N. M., Ahn, J. & Strano, M. S. A Pharmacokinetic Model of a Tissue Implantable Insulin Sensor. *Advanced Healthcare Materials*, n/a-n/a, doi:10.1002/adhm.201400264 (2014).
- 17 Hong, G. *et al.* Through-skull fluorescence imaging of the brain in a new near-infrared window. *Nat Photon* **8**, 723-730, doi:10.1038/nphoton.2014.166

<http://www.nature.com/nphoton/journal/v8/n9/abs/nphoton.2014.166.html#supplementary-information> (2014).

- 18 Iverson, N. M. *et al.* In vivo biosensing via tissue-localizable near-infrared-fluorescent single-walled carbon nanotubes. *Nat Nano* **8**, 873-880, doi:10.1038/nnano.2013.222

<http://www.nature.com/nnano/journal/v8/n11/abs/nnano.2013.222.html#supplementary-information> (2013).

- 19 Robinson, J. T. *et al.* In Vivo Fluorescence Imaging in the Second Near-Infrared Window with Long Circulating Carbon Nanotubes Capable of Ultrahigh Tumor Uptake. *Journal of the American Chemical Society* **134**, 10664-10669, doi:10.1021/ja303737a (2012).

- 20 Liu, Z., Tabakman, S., Welsher, K. & Dai, H. Carbon nanotubes in biology and medicine: In vitro and in vivo detection, imaging and drug delivery. *Nano Res.* **2**, 85-120, doi:10.1007/s12274-009-9009-8 (2009).

- 21 Welsher, K. *et al.* A route to brightly fluorescent carbon nanotubes for near-infrared imaging in mice. *Nat Nano* **4**, 773-780, doi:http://www.nature.com/nnano/journal/v4/n11/suppinfo/nnano.2009.294_S1.html (2009).

- 22 Kam, N. W. S., O'Connell, M., Wisdom, J. A. & Dai, H. Carbon nanotubes as multifunctional biological transporters and near-infrared agents for selective cancer cell destruction. *Proceedings of the National Academy of Sciences of the United States of America* **102**, 11600-11605, doi:10.1073/pnas.0502680102 (2005).

- 23 Heller, D. A. *et al.* Optical Detection of DNA Conformational Polymorphism on Single-Walled Carbon Nanotubes. *Science* **311**, 508-511, doi:10.1126/science.1120792 (2006).

- 24 Jeng, E. S., Moll, A. E., Roy, A. C., Gastala, J. B. & Strano, M. S. Detection of DNA Hybridization Using the Near-Infrared Band-Gap Fluorescence of Single-Walled Carbon Nanotubes. *Nano Letters* **6**, 371-375, doi:10.1021/nl051829k (2006).
- 25 Yang, R. *et al.* Noncovalent Assembly of Carbon Nanotubes and Single-Stranded DNA: An Effective Sensing Platform for Probing Biomolecular Interactions. *Analytical Chemistry* **80**, 7408-7413, doi:10.1021/ac801118p (2008).
- 26 Ahn, J.-H. *et al.* Label-Free, Single Protein Detection on a Near-Infrared Fluorescent Single-Walled Carbon Nanotube/Protein Microarray Fabricated by Cell-Free Synthesis. *Nano Letters* **11**, 2743-2752, doi:10.1021/nl201033d (2011).
- 27 Reuel, N. F. *et al.* Emergent Properties of Nanosensor Arrays: Applications for Monitoring IgG Affinity Distributions, Weakly Affined Hypermannosylation, and Colony Selection for Biomanufacturing. *ACS Nano* **7**, 7472-7482, doi:10.1021/nn403215e (2013).
- 28 Zhang, J. *et al.* A Rapid, Direct, Quantitative, and Label-Free Detector of Cardiac Biomarker Troponin T Using Near-Infrared Fluorescent Single-Walled Carbon Nanotube Sensors. *Advanced Healthcare Materials* **3**, 412-423, doi:10.1002/adhm.201300033 (2014).
- 29 Reuel, N. F. *et al.* Transduction of Glycan–Lectin Binding Using Near-Infrared Fluorescent Single-Walled Carbon Nanotubes for Glycan Profiling. *Journal of the American Chemical Society* **133**, 17923-17933, doi:10.1021/ja2074938 (2011).
- 30 Cha, T.-G. *et al.* Optical Nanosensor Architecture for Cell-Signaling Molecules Using DNA Aptamer-Coated Carbon Nanotubes. *ACS Nano* **5**, 4236-4244, doi:10.1021/nn201323h (2011).

- 31 Kruss, S. *et al.* Neurotransmitter Detection Using Corona Phase Molecular Recognition on Fluorescent Single-Walled Carbon Nanotube Sensors. *Journal of the American Chemical Society* **136**, 713-724, doi:10.1021/ja410433b (2013).
- 32 Barone, P. W. & Strano, M. S. Reversible Control of Carbon Nanotube Aggregation for a Glucose Affinity Sensor. *Angewandte Chemie* **118**, 8318-8321, doi:10.1002/ange.200603138 (2006).
- 33 Barone, P. W. & Strano, M. S. Single Walled Carbon Nanotubes as Reporters for the Optical Detection of Glucose. *Journal of Diabetes Science and Technology* **3**, 242-252, doi:10.1177/193229680900300204 (2009).
- 34 Mu, B. *et al.* A Structure–Function Relationship for the Optical Modulation of Phenyl Boronic Acid-Grafted, Polyethylene Glycol-Wrapped Single-Walled Carbon Nanotubes. *Journal of the American Chemical Society* **134**, 17620-17627, doi:10.1021/ja307085h (2012).
- 35 Yum, K. *et al.* Boronic Acid Library for Selective, Reversible Near-Infrared Fluorescence Quenching of Surfactant Suspended Single-Walled Carbon Nanotubes in Response to Glucose. *ACS Nano* **6**, 819-830, doi:10.1021/nn204323f (2011).
- 36 Yoon, H. *et al.* Periplasmic Binding Proteins as Optical Modulators of Single-Walled Carbon Nanotube Fluorescence: Amplifying a Nanoscale Actuator. *Angewandte Chemie* **123**, 1868-1871, doi:10.1002/ange.201006167 (2011).
- 37 Heller, D. A. *et al.* Multimodal optical sensing and analyte specificity using single-walled carbon nanotubes. *Nat Nano* **4**, 114-120, doi:http://www.nature.com/nnano/journal/v4/n2/supinfo/nnano.2008.369_S1.html (2009).

- 38 Giraldo, J. P. *et al.* Plant nanobionics approach to augment photosynthesis and biochemical sensing. *Nat Mater* **13**, 400-408, doi:10.1038/nmat3890
<http://www.nature.com/nmat/journal/v13/n4/abs/nmat3890.html#supplementary-information>
(2014).
- 39 Jin, H. *et al.* Detection of single-molecule H₂O₂ signalling from epidermal growth factor receptor using fluorescent single-walled carbon nanotubes. *Nat Nano* **5**, 302-309,
doi:http://www.nature.com/nnano/journal/v5/n4/suppinfo/nnano.2010.24_S1.html
(2010).
- 40 Kim, J.-H. *et al.* A Luciferase/Single-Walled Carbon Nanotube Conjugate for Near-Infrared Fluorescent Detection of Cellular ATP. *Angewandte Chemie* **122**, 1498-1501,
doi:10.1002/ange.200906251 (2010).
- 41 Zhang, J. *et al.* Single Molecule Detection of Nitric Oxide Enabled by d(AT)₁₅ DNA Adsorbed to Near Infrared Fluorescent Single-Walled Carbon Nanotubes. *Journal of the American Chemical Society* **133**, 567-581, doi:10.1021/ja1084942 (2010).
- 42 Zhang, J. *et al.* Molecular recognition using corona phase complexes made of synthetic polymers adsorbed on carbon nanotubes. *Nat Nano* **8**, 959-968,
doi:10.1038/nnano.2013.236
[http://www.nature.com/nnano/journal/v8/n12/abs/nnano.2013.236.html#supplementary-](http://www.nature.com/nnano/journal/v8/n12/abs/nnano.2013.236.html#supplementary-information)
[information](http://www.nature.com/nnano/journal/v8/n12/abs/nnano.2013.236.html#supplementary-information) (2013).
- 43 Liu, Z., Tabakman, S. M., Chen, Z. & Dai, H. Preparation of carbon nanotube bioconjugates for biomedical applications. *Nat. Protocols* **4**, 1372-1381 (2009).
- 44 Yan, L. Y., Poon, Y. F., Chan-Park, M. B., Chen, Y. & Zhang, Q. Individually Dispersing Single-Walled Carbon Nanotubes with Novel Neutral pH Water-Soluble

- Chitosan Derivatives. *The Journal of Physical Chemistry C* **112**, 7579-7587, doi:10.1021/jp711039s (2008).
- 45 Brege, J. J., Gallaway, C. & Barron, A. R. Fluorescence Quenching of Single-Walled Carbon Nanotubes with Transition-Metal Ions. *The Journal of Physical Chemistry C* **113**, 4270-4276, doi:10.1021/jp808667b (2009).
- 46 Hersam, M. C. Progress towards monodisperse single-walled carbon nanotubes. *Nat Nano* **3**, 387-394 (2008).
- 47 Liu, H., Nishide, D., Tanaka, T. & Kataura, H. Large-scale single-chirality separation of single-wall carbon nanotubes by simple gel chromatography. *Nat Commun* **2**, 309, doi:http://www.nature.com/ncomms/journal/v2/n5/supinfo/ncomms1313_S1.html (2011).
- 48 Moshhammer, K., Hennrich, F. & Kappes, M. Selective suspension in aqueous sodium dodecyl sulfate according to electronic structure type allows simple separation of metallic from semiconducting single-walled carbon nanotubes. *Nano Res.* **2**, 599-606, doi:10.1007/s12274-009-9057-0 (2009).
- 49 Tvrdy, K. *et al.* A Kinetic Model for the Deterministic Prediction of Gel-Based Single-Chirality Single-Walled Carbon Nanotube Separation. *ACS Nano* **7**, 1779-1789, doi:10.1021/nn305939k (2013).
- 50 Jain, R. M., Tvrdy, K., Han, R., Ulissi, Z. & Strano, M. S. Quantitative Theory of Adsorptive Separation for the Electronic Sorting of Single-Walled Carbon Nanotubes. *ACS Nano* **8**, 3367-3379, doi:10.1021/nn4058402 (2014).
- 51 Nelson, A. L., Dhimolea, E. & Reichert, J. M. Development trends for human monoclonal antibody therapeutics. *Nat Rev Drug Discov* **9**, 767-774 (2010).

- 52 Carter, P. J. Potent antibody therapeutics by design. *Nat Rev Immunol* **6**, 343-357, doi:http://www.nature.com/nri/journal/v6/n5/supinfo/nri1837_S1.html (2006).
- 53 Borrebaeck, C. A. K. Antibodies in diagnostics – from immunoassays to protein chips. *Immunology Today* **21**, 379-382, doi:[http://dx.doi.org/10.1016/S0167-5699\(00\)01683-2](http://dx.doi.org/10.1016/S0167-5699(00)01683-2) (2000).
- 54 Brennan, D. J., O'Connor, D. P., Rexhepaj, E., Ponten, F. & Gallagher, W. M. Antibody-based proteomics: fast-tracking molecular diagnostics in oncology. *Nat Rev Cancer* **10**, 605-617 (2010).
- 55 El-Sayed, I. H., Huang, X. & El-Sayed, M. A. Surface Plasmon Resonance Scattering and Absorption of anti-EGFR Antibody Conjugated Gold Nanoparticles in Cancer Diagnostics: Applications in Oral Cancer. *Nano Letters* **5**, 829-834, doi:10.1021/nl050074e (2005).
- 56 Ogi, H. *et al.* Concentration dependence of IgG–protein A affinity studied by wireless-electrodeless QCM. *Biosensors and Bioelectronics* **22**, 3238-3242, doi:<http://dx.doi.org/10.1016/j.bios.2007.03.003> (2007).
- 57 Saha, K., Bender, F. & Gizeli, E. Comparative Study of IgG Binding to Proteins G and A: Nonequilibrium Kinetic and Binding Constant Determination with the Acoustic Waveguide Device. *Analytical Chemistry* **75**, 835-842, doi:10.1021/ac0204911 (2003).
- 58 Schwartz, M. P., Alvarez, S. D. & Sailor, M. J. Porous SiO₂ Interferometric Biosensor for Quantitative Determination of Protein Interactions: Binding of Protein A to Immunoglobulins Derived from Different Species. *Analytical Chemistry* **79**, 327-334, doi:10.1021/ac061476p (2006).

- 59 Surolia, A., Pain, D. & Islam Khan, M. Protein A: nature's universal anti-antibody. *Trends in Biochemical Sciences* **7**, 74-76, doi:[http://dx.doi.org/10.1016/0968-0004\(82\)90082-2](http://dx.doi.org/10.1016/0968-0004(82)90082-2) (1982).
- 60 Nieba, L., Krebber, A. & Plückthun, A. Competition BIAcore for Measuring True Affinities: Large Differences from Values Determined from Binding Kinetics. *Analytical Biochemistry* **234**, 155-165, doi:<http://dx.doi.org/10.1006/abio.1996.0067> (1996).
- 61 Deisenhofer, J. Crystallographic refinement and atomic models of a human Fc fragment and its complex with fragment B of protein A from *Staphylococcus aureus* at 2.9- and 2.8-Å resolution. *Biochemistry* **20**, 2361-2370, doi:10.1021/bi00512a001 (1981).
- 62 Hanson, D. C. & Schumaker, V. N. A model for the formation and interconversion of protein A-immunoglobulin G soluble complexes. *The Journal of Immunology* **132**, 1397-1409 (1984).
- 63 Stevens, F. J. Modification of an Elisa-Based procedure for affinity determination: correction necessary for use with bivalent antibody. *Molecular Immunology* **24**, 1055-1060, doi:[http://dx.doi.org/10.1016/0161-5890\(87\)90073-3](http://dx.doi.org/10.1016/0161-5890(87)90073-3) (1987).
- 64 Wang, Z.-X. & Jiang, R.-F. A novel two-site binding equation presented in terms of the total ligand concentration. *FEBS Letters* **392**, 245-249, doi:[http://dx.doi.org/10.1016/0014-5793\(96\)00818-6](http://dx.doi.org/10.1016/0014-5793(96)00818-6) (1996).
- 65 EVANS, H. M., UYEI, N. & BARTZ, Q. R. THE PURIFICATION OF THE ANTERIOR PITUITARY GROWTH HORMONE BY FRACTIONATION WITH AMMONIUM SULFATE. *Endocrinology* **22**, 483-492, doi:doi:10.1210/endo-22-4-483 (1938).

- 66 MARX, W., SIMPSON, M. E. & EVANS, H. M. BIOASSAY OF THE GROWTH HORMONE OF THE ANTERIOR PITUITARY. *Endocrinology* **30**, 1-10, doi:doi:10.1210/endo-30-1-1 (1942).
- 67 GROESBECK, M. D. & PARLOW, A. F. Highly Improved Precision of the Hypophysectomized Female Rat Body Weight Gain Bioassay for Growth Hormone by Increased Frequency of Injections, Avoidance of Antibody Formation, and Other Simple Modifications. *Endocrinology* **120**, 2582-2590, doi:doi:10.1210/endo-120-6-2582 (1987).
- 68 Roswall, E. C. *et al.* Novel Assays Based on Human Growth Hormone Receptor as Alternatives to the Rat Weight Gain Bioassay for Recombinant Human Growth Hormone. *Biologicals* **24**, 25-39, doi:<http://dx.doi.org/10.1006/biol.1996.0003> (1996).
- 69 Reuel, N. F. *Label-free Carbon Nanotube Sensors for Glycan and Protein Detection* Ph.D. thesis, Massachusetts Institute of Technology, (2014).
- 70 Wang, L., Wei, L., Chen, Y. & Jiang, R. Specific and reversible immobilization of NADH oxidase on functionalized carbon nanotubes. *Journal of Biotechnology* **150**, 57-63, doi:<http://dx.doi.org/10.1016/j.jbiotec.2010.07.005> (2010).